Inferring the evolutionary history of the Sino-Himalayan biodiversity hotspot using Bayesian phylodynamics

Bethany J. Allen[1,2,*], Timothy G. Vaughan[1,2], Louis du Plessis[1,2], Thomas L. A. Schouten[3], Zili Yuan[4,5], Sean D. Willett[3], Tanja Stadler[1,2]

1 Department of Biosystems Science and Engineering, ETH Zurich, Klingelbergstrasse 48, 4056 Basel, Switzerland

2 Computational Evolution Group, Swiss Institute of Bioinformatics, Quartier Sorge, Bâtiment Amphipôle, 1015 Lausanne, Switzerland

3 Geological Institute, Department of Earth Sciences, ETH Zurich, Sonneggstrasse 5, 8092 Zurich, Switzerland

4 Swiss Federal Institute for Forest, Snow and Landscape Research (WSL), Zürcherstrasse 111, 8903 Birmensdorf, Switzerland

5 Department of Environmental System Science, ETH Zurich, Universitätstrasse 16, 8092 Zurich, Switzerland

* Corresponding author email: bethany.allen@bsse.ethz.ch

Abstract

The current status of the Sino-Himalayan region as a biodiversity hotspot, particularly for flora, has often been linked to the uplift of the Sino-Tibetan Plateau and Himalayan and Hengduan Mountains. However, the relationship between the topological development of the region and the onset of diversification is yet to be confirmed. Here, we apply Bayesian phylodynamic methods to a large phylogeny of angiosperm species from the Sino-Himalayas, to infer changes in their evolutionary rates through time. We find strong evidence for high diversification rates in the Paleocene, late Miocene and Pliocene, and for negative diversification rates in the Quaternary, driven by an increase in extinction rates. Our analyses suggest that changes in global palaeotemperatures are unlikely to be a driving force for these rate shifts. Instead, recovery after the end-Cretaceous mass extinction, the collision of the Indian continent with Eurasia and coeval topographic change in the Sino-Himalayans, and the impact of Pleistocene glaciations on this altitudinally-variable region may shape these rates. We also demonstrate the strong influence of change time choice on piecewise-constant trajectories in Bayesian phylodynamics, and advocate for the use of prior information when making this decision.

Introduction

The Sino-Himalayan region is likely the world's oldest and most biodiverse truly cold region, and is therefore probably also the place of origin of many clades of cold-adapted plants (Hagen et al. 2019; Ding et al. 2020). In particular, the Hengduan Mountains to the southeast of the region are home to a floral biodiversity hotspot (Sherman et al. 2008; Xing and Ree 2017; Ding et al. 2020). The region has a particularly large number of endemic plant species, and beta diversity is high, meaning that the taxonomic constituents of floral communities are highly variable across space (Sherman et al. 2008). Despite its age as a cold region, the Sino-Himalayas also contains angiosperm clades which have diverged more recently on average than the rest of China, with lower phylogenetic diversity (Lu et al. 2018). Collectively, this suggests that high diversification rates have likely been maintained across most of the Cenozoic here.

The accrual of so much plant diversity in the Sino-Himalayas has previously been attributed to the region's extreme altitudinal heterogeneity (Sherman et al. 2008; Liu et al. 2013; Favre et al. 2015). Geological dynamism is increasingly being recognised as a key driver behind many of the world's biodiversity hotspots (Hoorn et al. 2013; Antonelli et al. 2018; Pellissier et al. 2018; Chang et al. 2023), with the process of mountain uplift being linked to plant diversification around the world (Hughes and Atchison 2015; Steinbauer et al. 2016; Antonelli et al. 2018). Complex topography increases abiotic variability, which can result in rapid speciation as existing biotas adapt to these newly arising habitats (Hoorn et al. 2013; Hughes and Atchison 2015; Huang et al. 2019). Isolated mountain tops and poor connectivity between similar habitats limits dispersal and facilitates local adaptation, further promoting allopatric speciation and endemism (Hoorn et al. 2013; Steinbauer et al. 2016; Dool et al. 2022). The existence of strong environmental gradients with altitude, across a relatively small area, may also allow migration to track suitable habitat in the face of climate change (Hoorn et al. 2013; Huang et al. 2019). During glacial activity in the Quaternary, many plants were driven into refugia, which separated populations and thereby contributed to genetic divergence and allopatric speciation, as well as extinction (Liu et al. 2013; Hughes and Atchison 2015; Steinbauer et al. 2016). However, the Sino-Himalayas is one of the lesser-studied and least understood mountainous regions of the world, with the relationship between uplift and biodiversity yet to be clearly demonstrated (Favre et al. 2015; Xing and Ree 2017).

The region has experienced considerable topographic change over the Cenozoic, mostly linked to the convergence and eventual collision of the Indian and Eurasian continents (e.g. Yin and Harrison 2000; Royden et al. 2008; Kapp and Decelles 2019; Spicer et al. 2021; Ding et al. 2022). Uplift has also had a fundamental role in the development of the East Asian monsoon, a major component of the local climate regime (Farnsworth et al. 2019). The exact nature of the geological processes involved, and the timing of these events, remain unresolved (Royden et al. 2008; Kapp and Decelles 2019; Spicer et al. 2021; Ding et al. 2022). While stable isotope palaeoaltimetry is the most commonly used method for reconstructing palaeoaltitude, there are many other factors that can affect these isotope ratios which may dilute or obscure the altitudinal signal (Huang et al. 2019; Spicer et al. 2021).

Uncertainty in the topographical and climatic history of the region is a major barrier to directly linking biodiversification to mountain building (Hughes and Atchison 2015; Favre et al. 2015; Xing and Ree 2017; Antonelli et al. 2018). Relating mountain building to biodiversity often requires considering thresholds, such as the point at which mountains became high enough to interact with climate systems (Huang et al. 2019), or extend above the tree line (Ding et al. 2020), but our knowledge of the placement of these thresholds is limited, let alone when they were crossed. In the Sino-Himalayas, the timing of the development of a land bridge between Eurasia and India likely also had strong impacts on the extent of biotic interchange between the

two regions (Spicer et al. 2021). Many of these phenomena will have been inconsistent across space, influencing different subregions within the Sino-Himalayas at different times. The scale-dependence of both biotic and abiotic variables also complicates efforts towards comparison (Antonelli et al. 2018).

There are also complexities in reconstructing biodiversification, i.e. the history of evolutionary rates, in the region. Occurrence-based information describing plant distributions and richness are valuable, but likely to be incomplete (Kreft and Jetz 2007), and are difficult to compare between the present and the fossil record due to contrasting sampling biases. Phylogenetic approaches aim to infer the evolutionary relationships between species, and can provide insight into the timing of speciation and extinction events. Such approaches have previously been used to infer the evolutionary history of Sino-Himalayan plants, but only within individual subclades, meaning that any results are taxon-specific and often can only encompass fairly shallow geological time (Favre et al. 2015; Xing and Ree 2017).

Here, we use phylodynamic models implemented in the Bayesian phylogenetics framework BEAST 2 (Bouckaert et al. 2019) to infer evolutionary rates from a previously constructed phylogeny of extant Sino-Himalayan angiosperm species (Liu et al. 2021). The high taxonomic resolution, large size and geographic restriction of the phylogeny makes it ideal for inferring angiosperm speciation and extinction rates within the region. We use a birth-death skyline model (Stadler et al. 2012) to infer piecewise-constant rates for set intervals throughout the Cenozoic. We then compare these rates to contemporaneous global palaeotemperatures, to examine the extent to which global versus local drivers are likely to have influenced the inferred rates.

The potential nonidentifiability of evolutionary rates based on extant phylogenies has recently become a topic of fierce debate (Louca and Pennell 2020; Legried and Terhorst 2022; Morlon et al. 2022; Kopperud et al. 2023). Louca and Pennell (2020) describe how speciation and extinction functions are drawn from congruence classes, within which each pair of functions is equally likely to fit the evolutionary history of a given phylogeny. As a result, it may not be possible to discern which of these pairs of functions truly generated the observed phylogeny. Legried and Terhorst (2022) demonstrate that piecewise-constant rates, such as those we infer here, are identifiable under certain conditions. But regardless, it seems prudent to conduct our analyses in a way which is mindful of this debate. Here, we implement a number of steps to thoroughly interrogate our model and our results, including testing the influence of prior choice, verifying model adequacy, and investigating common trends in the rate functions contained in the posterior.

Methods

Phylogeny

Liu et al. (2021) built a large maximum likelihood phylogeny of extant angiosperms currently found in the Sino-Himalayas and surrounding regions, excluding recent introductions. Their phylogeny included 19,313 species, with genetic data available for 8,864 of these tips. They time-scaled their phylogeny using node calibrations, at 123 calibration points sourced from previous literature. We chose this as the most appropriate phylogeny to conduct our phylodynamic analyses on due to (1) its large number of tips, (2) its wide taxonomic breadth, allowing evolutionary rates to be inferred for all angiosperms collectively and resulting in a root age in the Early Cretaceous, therefore allowing us to infer rates for the whole of the Cenozoic, (3) its restriction to our geographic region of interest, and (4) its use of species at the tips, as this is the taxonomic resolution at which the processes in our model are assumed to operate.

Prior to our analyses, we pruned all tips from the tree which were not associated with any genetic data, as the phylogenetic placement and associated branching times of these tips are less reliable.

Birth-death skyline

Bayesian birth-death skyline inference (Meredith et al. 2011; Stadler 2011; Stadler et al. 2012; Heath et al. 2014) was undertaken based on the 8,864-tip fixed phylogeny using the BDSKY package in BEAST2 (Bouckaert et al. 2019). The model was parameterised using birth (speciation, λ) and death (extinction, μ) rates, both quantified per branch per million years and allowed to change in a piecewise-constant fashion, and an extant sampling probability (ρ). For both speciation and extinction rates, an exponential prior with a mean of 1.0 was used, placing most probability on smaller rates, up to a magnitude observed across species phylogenies of a wide range of taxa (Henao Diaz et al. 2019).

To account for uncertainty in the true number of extant angiosperm species in the Sino-Himalayas, the extant sampling probability prior was set using two different approaches, both based on the proportion of tips with genetic data in the Liu et al. (2021) phylogeny (45.9%). Firstly, the sampling prior was defined using a beta distribution (α = 4, β = 8). Secondly, separate analyses were run using three fixed sampling levels of 0.5 (high completeness), 0.3 (mid completeness) and 0.1 (low completeness). The change times for the piecewise constant rates were also defined using two different regimes. Firstly, 14 equally-spaced bins were used, each 10My in duration. Secondly, change times were placed at the boundaries of recognised geological intervals, to create 13 temporal bins (Table 1). Eight separate MCMC chains, one for each combination of the two sets of change times and four sets of sampling priors, were run until they reached convergence (ESS values for all parameters over 200 after the removal of a 10% burn-in).

Quantifying change

Post-processing of the BDSKY log files was conducted using R (R Core Team 2023). Net diversification ($\lambda_i - \mu_i$) rates were calculated *post hoc* for each iteration of the MCMC chains. Median values were then calculated for all parameters in each time interval, alongside 95% highest posterior density (HPD) values using the R package coda (Plummer et al. 2020). We also calculated the numerical difference in each inferred rate across each pair of adjacent time bins within an iteration of the MCMC chain. This allowed us to summarise the posterior distribution of rate trajectories in the posterior, particularly whether rates tended to increase or decrease consistently across a temporal boundary.

Model adequacy

In order to verify the performance of our model, we simulated phylogenies using the inferred parameters from the BDSKY analysis and re-analysed them Duchêne et al. (2019). The median inferred birth and death trajectories were used to generate phylogenies using a birth-death model in the BEAST2 package ReMASTER (Vaughan 2023). After 140My (at the “present”), phylogenies which did not reach the number of tips in the total Liu et al. (2021) phylogeny were discarded, and 8,864 tips were selected at random to constitute the “sampled” phylogeny. The number of discarded tips (and hence the sampling proportion) was also recorded. This process was repeated until 100 phylogenies had been generated. Each of these phylogenies was then analysed using the same BDSKY birth-death skyline model as the original analyses, to investigate the accuracy with which the true, generative rate functions could be recovered.

Palaeotemperature comparison

Scotese et al. (2021) produced estimates of global average temperature for each 1My interval of the Phanerozoic by combining oxygen isotope data and information from lithological indicators. We tested for a possible relationship between our inferred rates and these global palaeotemperatures, to rule out temperature as a major driver of the (local) Sino-Himalayan diversity trends. We calculated the maximum, minimum and mean temperature estimate across the 1My intervals included in each time bin (boundary years were included in both bins). We then used linear regression to test for correlations between the mean global temperature estimates and evolutionary rate estimates (speciation, extinction, and net diversification) for each iteration of our MCMC posteriors, and summarised the R^2 and p-values across these tests.

Results

Reconstructed patterns of net diversification in Sino-Himalayan angiosperms were highly similar regardless of the sampling prior used (Figure S1). The different fixed sampling proportion priors changed the absolute amplitude of speciation and extinction rates, but not the shape of their trajectories, and hence diversification rate estimates remained comparable regardless of which sampling prior was used. As a result, the main text figures present the analyses carried out using the beta sampling proportion prior. The model adequacy analyses also recovered posteriors with median rate values close to those used to simulate the phylogenies (Figure S2), despite incorporating a range of sampling proportions. This provides further evidence that the results obtained here are identifiable (Duchêne et al. 2019).

The overall trends of speciation and extinction were also broadly comparable between the different change times used (Figure 1). Median estimates of speciation and extinction were relatively constant throughout the Cenozoic, with speciation rates typically around 0.5 per branch per million years, and extinction rates around 0.4 per branch per million years. The analysis using equally-spaced time bins suggests that both rates may have increased over the last 50My, however this is not seen in the analysis using geological time bins.

In both analyses, net diversification was highest in the Early Cretaceous and gradually fell until 100My ago, since which it has remained relatively constant (Figure 1). The analysis with equally-spaced time bins does not indicate any strong shifts in diversification rate, with over 95% of the posterior distribution indicating a positive diversification rate between 140 and 120Ma, 50 and 20Ma, and over the last 10Ma. This analysis has relatively wide 95% HPD intervals throughout, while in contrast, the analysis using geological time bins has generally narrower 95% HPD intervals, and indicates bigger shifts in diversification rate. For example, diversification rates are estimated to be near-zero during the latest Cretaceous, but are considerably higher in the Paleocene, with 99.73% of the posterior indicating a positive diversification rate at this time. Diversification then falls back to near-zero values in the early Eocene. Diversification rates are also estimated to be positive during the late Miocene and Pliocene, with 99.89% and 99.97% of the posterior above 0 respectively. However, during the Quaternary, a negative diversification rate is recovered in all iterations.

The direction and magnitude of rate shifts across change times in each individual iteration was also calculated (Figure 2), to quantify the posterior support for observed trends over time. Using the equally-spaced time bins, most interval transitions resulted in an approximately even number of increases and decreases in speciation, extinction and net diversification rates across iterations. An increase in both speciation rates and extinction rates is recovered in the majority of iterations at the 30Mya (99.65% for speciation, 98.24% for extinction) and 20Mya (97.13% for

speciation, 98.82% for extinction) boundaries, the latter associated with a negative diversification rate (in 98.56% of iterations). Speciation and extinction rates both fell in 96.71% of iterations at the 10Mya boundary. The width of the HPDs tended to increase with the age of the boundary time. Using the geological time bins, the direction of diversification rate shifts between bins was more consistent across iterations. 97.58% of iterations indicated a fall in diversification rate between the early Lower and late Lower Cretaceous, and 96.05% recovered another fall in the middle of the Cretaceous. In 99.73% of iterations, an increase in diversification rates across the Cretaceous-Paleocene (K-Pg) was estimated, and 95.62% also recovered a fall in diversification rates into the early Eocene. 96.77% of the iterations showed an increase in diversification rate from the late Miocene into the Pliocene, and all showed a fall in diversification rate into the Quaternary, accompanied by a near-universal (99.98%) increase in extinction rates.

The relationships between global average palaeotemperatures and the estimated evolutionary rates are summarised in Figure 3. For the equally-spaced time bins, both speciation and extinction rates appear to have a weak, negative correlation with global palaeotemperature, but no clear patterns arise for any of the other analyses. To investigate this quantitatively, the relationship between the mean palaeotemperature for each time bin and the rate trajectories for each iteration in the Bayesian analysis was tested using linear regression, the results of which are shown in Figure 4. For the equally-spaced time bins, 60.4% and 58.1% of speciation and extinction rate trajectories respectively had a p-value below 0.05, with median R^2 values of 0.380 and 0.347. Less than 0.001% of diversification trajectories had a statistically significant relationship (at the 0.05 level) with palaeotemperature, and the median R^2 value was 0.004. The regression analyses showed less evidence of a relationship between evolutionary rates and palaeotemperature when using the geological time bins (median speciation R^2 = 0.128, p-values below 0.05 = 26.0%; median extinction R^2 = 0.100, p-values below 0.05 = 19.0%; median diversification R^2 = 0.028, p-values below 0.05 $<$ 0.001%).

Discussion

Our phylodynamic analyses, particularly across geological time intervals, reveal multiple strong shifts in diversification rates for angiosperms in the Sino-Himalayas (Figure 1, 2). We see high diversification rates in the early history of the group, during the Early Cretaceous, accompanied by the greatest uncertainty in speciation and extinction rates; this is commonly observed in phylogenetic analyses of diversification rates through time (Henao Diaz et al. 2019). Positive diversification rates are also inferred in the Paleocene, late Miocene and Pliocene. Although near-zero diversification rates are inferred for several intervals, the only time bin with clearly negative diversification rates is the Quaternary, driven by an increase in extinction rates.

Our comparison of global palaeotemperatures and evolutionary rates provide some evidence of a negative correlation between palaeotemperature and speciation and extinction rates in Sino-Himalayan angiosperms when using equally-spaced time intervals. The direction of this relationship is unusual, as higher temperatures are usually linked to higher speciation and diversification rates (Allen et al. 2006). However, most of the plants which inhabit the Sino-Himalayas evolved at high altitudes and are adapted to cold conditions; it may be the case that geological intervals with colder temperatures expanded the area available for these plants to inhabit, and potentially facilitated their further diversification (Ding et al. 2020). Heightened extinction rates in colder times are perhaps more expected; in this region, the loss of habitable area due to glaciation at high altitudes as temperatures fell may also be important. However, substantially less support was found for a correlation between diversification rates and palaeotemperature, and this was also the case for all evolutionary rates when using geological

time bins. As a result, the link between global palaeotemperatures and evolutionary rates in Sino-Himalayan angiosperms appears tenuous. These analyses suggest that the diversification rate shifts we infer were not driven by global palaeotemperature, but may instead have been driven by topographic and climatic shifts associated with the progressive uplift of the Sino-Himalayan region over the Cenozoic. High levels of uncertainty about the timing and nature of uplift across the Sino-Himalayas obstruct our ability to link evolutionary rate shifts with specific topographic changes, and also limit the accuracy and resolution of local palaeoclimate reconstructions. However, we discuss below some of the implications and possible drivers, at a coarse scale, for the key shifts we observed based on the analyses using geological time bins.

The severity of the end-Cretaceous mass extinction for angiosperms has been debated (McElwain and Punyasena 2007; Vajda and Bercovici 2014; Carvalho et al. 2021; Thompson and Ramírez-Barahona 2023), and we do not see substantially increased extinction rates in Sino-Himalayan angiosperms in the latest Cretaceous at this time. However, we do infer high diversification rates during the Paleocene, immediately following this event. The initial India-Eurasia collision is thought to have taken place in the Paleocene (DeCelles et al. 2014; Hu et al. 2015; Li et al. 2015; Najman et al. 2017), but there was considerable area of high topography uplifted in an Andean-type orogen that developed prior to collision (e.g. Murphy et al. 1997; Kapp and Decelles 2019), potentially driving angiosperm diversification. Biotic interchange is also likely to have commenced prior to the India-Eurasia collision, with increasing numbers of plant seeds crossing the ever-shortening distance between the two landmasses; this would create a signal of diversification in our phylogeny, introducing new species to the Sino-Himalayas from India. Many genome duplication events are also thought to have taken place in angiosperms around the K-Pg boundary (Vanneste et al. 2014; Lohaus and Peer 2016; Clark and Donoghue 2018); such events create more redundant genetic material, theoretically facilitating diversification and rapid adaptation to new environmental conditions, although this is controversial (Soltis et al. 2009; Estep et al. 2014; Vanneste et al. 2014; Lohaus and Peer 2016; Clark and Donoghue 2018). In this region, it is possible that the onset of drastic topographic change, coupled with increased genetic lability, drove increased angiosperm speciation rates during the Paleocene.

We also infer high diversification rates in the late Miocene and Pliocene. The late Miocene is thought to be when C4 grasses rose to dominance over C3 grasslands, again linked to a series of genome duplications in the clade (Estep et al. 2014; Lohaus and Peer 2016), and this general trend across angiosperms may have played a role in driving this Sino-Himalayan diversification. Recent reassessments of the timing of the uplift of the Hengduan Mountains also indicate that this may have taken place during the late Miocene to Pliocene (Xing and Ree 2017; Liu-Zeng et al. 2018). The Hengduan Mountains are the most florally diverse subregion (Sherman et al. 2008; Zhang et al. 2009; Liu et al. 2013), so we might expect that the uplift of this range would be one of the most influential tectonic events on angiosperm biodiversity. Our analyses also indicate that Sino-Himalayan angiosperms experienced high extinction rates, and negative diversification, in the Quaternary. Pleistocene glaciation, which was likely widespread across this high-altitude region, has previously been highlighted as a major driver of modern biodiversity patterns (Zhang et al. 2009; Zhan et al. 2011; Renner 2016).

Our phylodynamic analyses were not sensitive to the sampling probability prior. However, our comparison of using equally-spaced versus geological time bins demonstrates that the shape of evolutionary rate trajectories, and the subsequent conclusions drawn, can be highly influenced by change time placement. Equally-spaced time bins can be a reasonable choice in the absence of prior information about when evolutionary rates may have changed. But geological intervals are designated based on when we consider the Earth system to have been relatively

stable, with changes in its state in between; geological interval boundaries therefore represent a logical best guess for when evolutionary rate shifts may have occurred, particularly in clades which are highly sensitive to their environment. Some facets of our results also point towards better model fit when using the geological time bins, such as more consistent diversification rate trajectories between iterations, and narrower HPD intervals. Careful consideration of break points in piecewise-constant skylines is clearly necessary, but based on our results, geological time intervals seem the most appropriate choice for macroevolutionary studies, at least in the absence of alternative prior knowledge specific to the clade of interest.

The approach we chose to use here was to analyse a single, extant-only phylogeny. In contrast with other previous analyses of diversification rates in the Sino-Himalayan region, the size of our phylogeny allowed us to infer evolutionary rates throughout the whole of the Cenozoic, and therefore to assess the influence of a greater extent of uplift history on evolutionary rates. However, this approach also has its limitations. For example, we assume that the phylogeny we used, constructed by (Liu et al. 2021), is correct, or at least a close approximation. Although the phylogeny includes a large number of tips, it does not contain fossil tips, which means our results may be less reliable with increasing age from the present (Favre et al. 2015); this is already reflected in increased HPD interval widths for our older time bins. Yunnan has a particularly rich Cenozoic plant fossil record (Huang et al. 2016) which could provide more insight into the early evolutionary history of the clade. We hope in future to see the development of methods that combine greater phylogeny size, increased types of data that can be placed on the tips, and making maximal use of available age information (Stadler et al. 2018; Huang et al. 2019).

Although our analyses provide a clear picture of evolutionary trends across the whole Sino-Himalayan region, some previous studies have inferred rates at a higher biogeographic resolution, for the Qinghai-Tibetan Plateau, and the Himalayan and Hengduan Mountain ranges separately (Xing and Ree 2017; Ding et al. 2020). Such analyses with biogeographic structure can highlight which regions, and therefore which particular tectonic or topographic events, are likely to have driven specific evolutionary rate shifts (Favre et al. 2015). Given the scale of uncertainty about the timing of some of these events, it may also be possible that, assuming topographic change is the major driver of evolutionary rate shifts, such biogeographic analyses could instead help to improve our understanding of the sequence of tectonic events in the region (Huang et al. 2019). The aforementioned studies used methodological approaches which instead compromised on the length of time over which evolutionary rates could be inferred, and on the incorporation of sampling bias into their models. But frameworks such as the GeoSSE model (Goldberg et al. 2011) demonstrate how our model could be extended in future to increase the biogeographic resolution of our analyses.

Acknowledgements/Funding

This work was funded by an ETH+ grant (BECCY), which supported the contributions of BJA, TLAS, ZY, SDW and TS.

Author contributions

TS and SDW conceived the project. BJA and TS developed the analytical pipeline, with assistance from TGV and LdP. BJA conducted the analyses, produced the figures and drafted the manuscript. All authors contributed to discussion and editing the manuscript.

References

Allen, A. P., J. F. Gillooly, V. M. Savage, and J. H. Brown. 2006. Kinetic Effects of Temperature on Rates of Genetic Divergence and Speciation. *Proceedings of the National Academy of Sciences USA* 103 (24): 9130–35. https://doi.org/10.1073/pnas.0603587103.

Antonelli, A., W. D. Kissling, S. G. A. Flantua, M. A. Bermúdez, A. Mulch, A. N. Muellner-Riehl, H. Kreft, et al. 2018. Geological and Climatic Influences in Mountain Biodiversity. *Nature Geoscience* 11: 718–25. https://doi.org/10.1038/s41561-018-0236-z.

Bouckaert, R., T. G. Vaughan, J. Barido-Sottani, S. Duchêne, M. Fourment, A. Gavryushkina, J. Heled, et al. 2019. BEAST 2.5: An Advances Software Platform for Bayesian Evolutionary Analysis. *PLoS Computational Biology* 15 (4): e1006650. https://doi.org/10.1371/journal.pcbi.1006650.

Carvalho, M. R., C. Jaramillo, F. de la Parra, D. Caballero-Rodrígues, F. Herrera, S. Wing, B. L. Turner, et al. 2021. Extinction at the End-Cretaceous and the Origin of Modern Neotropical Rainforests. *Science* 372 (6537): 63–68. https://doi.org/10.1126/science.abf1969.

Chang, Y., K. Gelwick, S. D. Willett, X. Shen, C. Albouy, A. Luo, Z. Wang, N. E. Zimmermann, and L. Pellissier. 2023. Phytodiversity Is Associated with Habitat Heterogeneity from Eurasia to the Hengduan Mountains. *New Phytologist*. https://doi.org/10.1111/nph.19206.

Clark, J. W., and P. C. J. Donoghue. 2018. Whole-Genome Duplication and Plant Macroevolution. *Trends in Plant Science* 23 (10): 933–45. https://doi.org/10.1016/j.tplants.2018.07.006.

DeCelles, P. G., P. Kapp, G. E. Gehrels, and L. Ding. 2014. Paleocene-Eocene Foreland Basin Evolution in the Himalaya of Southern Tibet and Nepal: Implications for the Age of Initial India-Asia Collision. *Tectonics* 33 (5): 824–49. https://doi.org/10.1002/2014TC003522.

Ding, L., P. Kapp, F. Cai, C. N. Garzione, Z. Xiong, H. Wang, and C. Wang. 2022. Timing and Mechanisms of Tibetan Plateau Uplift. *Nature Reviews Earth & Environment* 3 (10): 652–67. https://doi.org/10.1038/s43017-022-00318-4.

Ding, W., R. H. Ree, R. A. Spicer, and Y. Xing. 2020. Ancient Orogenic and Monsoon-Driven Assembly of the World's Richest Temperate Alpine Flora. *Science* 369 (6503): 578–81. https://doi.org/10.1126/science.abb4484.

Dool, S. E., M. D. Picker, and M. J. B. Eberhard. 2022. Limited Dispersal and Local Adaptation Promote Allopatric Speciation in a Biodiversity Hotspot. *Molecular Ecology* 31 (1): 279–95. https://doi.org/https://doi.org/10.1111/mec.16219.

Duchêne, S., R. Bouckaert, D. A. Duchêne, T. Stadler, and A. J. Drummond. 2019. "Phylodynamic Model Adequacy Using Posterior Predictive Simulations." *Systematic Biology* 68 (2): 358–64. https://doi.org/10.1093/sysbio/syy048.

Estep, M. C., M. R. McKain, D. Vela Diaz, J. Zhong, J. G. Hodge, T. R. Hodkinson, D. J. Layton, S. T. Malcomber, R. Pasquet, and E. A. Kellogg. 2014. Allopolyploidy, Diversification, and the Miocene Grassland Expansion. *Proceedings of the National Academy of Sciences USA* 111 (42): 15149–54. https://doi.org/10.1073/pnas.1404177111.

Farnsworth, A., D. J. Lunt, S. A. Robinson, P. J. Valdes, W. H. G. Roberts, P. D. Clift, P. Marwick, et al. 2019. Past East Asian Monsoon Evolution Controlled by Paleogeography, Not CO2. *Science Advances* 5 (10): eaax1697. https://doi.org/10.1126/sciadv.aax1697.

Favre, A., M. Päckert, S. U. Pauls, S. C. Jähnig, D. Uhl, I. Michalak, and A. N. Muellner-Riehl. 2015. The Role of the Uplift of the Qinghai-Tibetan Plateau for the Evolution of Tibetan Biotas. *Biological Reviews* 90 (1): 236–53. https://doi.org/10.1111/brv.12107.

Gearty, W. 2023. *deeptime: plotting tools for anyone working in deep time.* R Package Version 1.0.1.

Goldberg, E. E., L. T. Lancaster, and R. H. Ree. 2011. Phylogenetic Inference of Reciprocal Effects Between Geographic Range Evolution and Diversification. *Systematic Biology* 60 (4): 451–65. https://doi.org/10.1093/sysbio/syr046.

Hagen, O., L. Vaterlaus, C. Albouy, A. Brown, F. Leugger, R. E. Onstein, C. Novaes de Santana, C. R. Scotese, and L. Pellissier. 2019. Mountain Building, Climate Cooling and the Richness of Cold-Adapted Plants in the Northern Hemisphere. *Journal of Biogeography* 46 (8): 1792–1807. https://doi.org/10.1111/jbi.13653.

Heath, T. A., J. P. Huelsenbeck, and T. Stadler. 2014. The Fossilized Birth-Death Process for Coherent Calibration of Divergence-Time Estimates. *Proceedings of the National Academy of Sciences USA* 111 (29): E2957–66. https://doi.org/10.1073/pnas.1319091111.

Henao Diaz, L. F., L. J. Harmon, M. T. C. Sugawara, E. T. Miller, and M. W. Pennell. 2019. Macroevolutionary Diversification Rates Show Time Dependency. *Proceedings of the National Academy of Sciences USA* 116 (15): 7403–8. https://doi.org/10.1073/pnas.1818058116.

Hoorn, C., V. Mosbrugger, A. Mulch, and A. Antonelli. 2013. Biodiversity from Mountain Building. *Nature Geoscience* 6: 154. https://doi.org/10.1038/ngeo1742.

Hu, X., E. Garzanti, T. Moore, and I. Raffi. 2015. Direct Stratigraphic Dating of India-Asia Collision Onset at the Selandian (Middle Paleocene, 59 ± 1 Ma). *Geology* 43 (10): 859–62. https://doi.org/10.1130/G36872.1.

Huang, S., M. J. M. Meijers, A. Eyres, A. Mulch, and S. A. Fritz. 2019. Unravelling the History of Biodiversity in Mountain Ranges Through Integrating Geology and Biogeography. *Journal of Biogeography* 46 (8): 1777–91. https://doi.org/10.1111/jbi.13622.

Huang, Y., L. Jia, Q. Wang, V. Mosbrugger, T. Utescher, T. Su, and Z. Zhou. 2016. Cenozoic Plant Diversity of Yunnan: A Review. *Plant Diversity* 38 (6): 271–82. https://doi.org/10.1016/j.pld.2016.11.004.

Hughes, C. E., and G. W. Atchison. 2015. The Ubiquity of Alpine Plant Radiations: From the Andes to the Hengduan Mountains. *New Phytologist* 207 (2): 275–82. https://doi.org/10.1111/nph.13230.

Kapp, P., and P. G. Decelles. 2019. Mesozoic–Cenozoic Geological Evolution of the Himalayan-Tibetan Orogen and Working Tectonic Hypotheses. *American Journal of Science* 319 (3): 159–254. https://doi.org/10.2475/03.2019.01.

Kopperud, B. T., A. F. Magee, and S. Höhna. 2023. Rapidly Changing Speciation and Extinction Rates Can Be Inferred in Spite of Nonidentifiability. *Proceedings of the National Academy of Sciences USA* 120 (7): e2208851120. https://doi.org/10.1073/pnas.2208851120.

Kreft, H., and W. Jetz. 2007. Global Patterns and Determinants of Vascular Plant Diversity. *Proceedings of the National Academy of Sciences USA* 104 (14): 5925–30. https://doi.org/10.1073/pnas.0608361104.

Legried, B., and J. Terhorst. 2022. A Class of Identifiable Phylogenetic Birth-Death Models. *Proceedings of the National Academy of Sciences USA* 119 (35): e2119513119. https://doi.org/10.1073/pnas.2119513119.

Li, J., X. Hu, E. Garzanti, W. An, and J. Wang. 2015. Paleogene Carbonate Microfacies and Sandstone Provenance (Gamba Area, South Tibet): Stratigraphic Response to Initial India–Asia Continental Collision. *Journal of Asian Earth Sciences*, Special issue on Development of the Asian Tethyan Realm, 104: 39–54. https://doi.org/10.1016/j.jseaes.2014.10.027.

Liu, J., M. Möller, J. Provan, L. Gao, R. Chandra Poudel, and D. Li. 2013. Geological and Ecological Factors Drive Cryptic Speciation of Yews in a Biodiversity Hotspot. *New Phytologist* 199 (4): 1093–1108. https://doi.org/10.1111/nph.12336.

Liu, Y., J. Ye, H. Hu, D. Peng, L. Zhao, L. Lu, W. Zaman, and Z. Chen. 2021. Influence of Elevation on Bioregionalisation: A Case Study of the Sino-Himalayan Flora. *Journal of Biogeography* 48 (10): 2578–87. https://doi.org/10.1111/jbi.14222.

Liu-Zeng, J., J. Zhang, D. McPhillips, P. Reiners, W. Wang, R. Pik, L. Zeng, et al. 2018. Multiple Episodes of Fast Exhumation Since Cretaceous in Southeast Tibet, Revealed by Low-Temperature Thermochronology. *Earth and Planetary Science Letters* 490: 62–76. https://doi.org/10.1016/j.epsl.2018.03.011.

Lohaus, R., and Y. Van de Peer. 2016. Of Dups and Dinos: Evolution at the k/Pg Boundary. *Current Opinion in Plant Biology* 30: 62–69. https://doi.org/10.1016/j.pbi.2016.01.006.

Louca, S., and M. W. Pennell. 2020. Extant Timetrees Are Consistent with a Myriad of Diversification Histories. *Nature* 580: 502–5. https://doi.org/10.1038/s41586-020-2176-1.

Lu, L., L. Mao, T. Yang, J. Ye, B. Liu, H. Li, M. Sun, et al. 2018. Evolutionary History of the Angiosperm Flora of China. *Nature* 554: 234–38. https://doi.org/10.1038/nature25485.

McElwain, J. C., and S. W. Punyasena. 2007. Mass Extinction Events and the Plant Fossil Record. *Trends in Ecology and Evolution* 22 (10): 548–57. https://doi.org/10.1016/j.tree.2007.09.003.

Meredith, R. W., J. E. Janečka, J. Gatesy, O. A. Ryder, C. A. Fisher, E. C. Teeling, A. Goodbla, et al. 2011. Impacts of the Cretaceous Terrestrial Revolution and KPg Extinction on Mammal Diversification. *Science* 334 (6055): 521–24. https://doi.org/10.1126/science.1211028.

Morlon, H., S. Robin, and F. Hartig. 2022. Studying Speciation and Extinction Dynamics from Phylogenies: Addressing Identifiability Issues. *Trends in Ecology and Evolution* 37 (6): 497–506. https://doi.org/10.1016/j.tree.2022.02.004.

Murphy, M. A., An Yin, T. M. Harrison, S. B. Dürr, Chen Z, F. J. Ryerson, W. S. F. Kidd, Wang X, and Zhou X. 1997. Did the Indo-Asian Collision Alone Create the Tibetan Plateau? *Geology* 25 (8): 719–22. https://doi.org/10.1130/0091-7613(1997)025<0719:DTIACA>2.3.CO;2.

Najman, Y., D. Jenks, L. Godin, M. Boudagher-Fadel, I. Millar, E. Garzanti, M. Horstwood, and L. Bracciali. 2017. The Tethyan Himalayan Detrital Record Shows That India–Asia Terminal Collision Occurred by 54 Ma in the Western Himalaya. *Earth and Planetary Science Letters* 459: 301–10. https://doi.org/10.1016/j.epsl.2016.11.036.

Pellissier, L., C. Heine, D. F. Rosauer, and C. Albouy. 2018. Are Global Hotspots of Endemic Richness Shaped by Plate Tectonics? *Biological Journal of the Linnean Society* 123 (1): 247–61. https://doi.org/10.1093/biolinnean/blx125.

Plummer, M., N. Best, K. Cowles, K. Vines, D. Sarkar, D. Bates, R. Almond, and A. Magnusson. 2020. *Coda: Output Analysis and Diagnostics for MCMC*. R Package Version 0.19-4.

R Core Team. 2023. *R: A Language and Environment for Statistical Computing*. Vienna, Austria: R Foundation for Statistical Computing. https://www.R-project.org/. Version 4.3.1.

Renner, S. S. 2016. Available Data Point to a 4-Km-High Tibetan Plateau by 40 Ma, but 100 Molecular-Clock Papers Have Linked Supposed Recent Uplift to Young Node Ages. *Journal of Biogeography* 43 (8): 1479–87. https://doi.org/10.1111/jbi.12755.

Royden, L. H., B. C. Burchfiel, and R. D. van der Hilst. 2008. The Geological Evolution of the Tibetan Plateau.*Science* 321 (5892): 1054–58. https://doi.org/10.1126/science.1155371.

Scotese, C. R., H. Song, B. J. W. Mills, and D. G. van der Meer. 2021. Phanerozoic Paleotemperatures: The Earth's Changing Climate During the Last 540 Million Years. *Earth-Science Reviews* 215: 103503. https://doi.org/10.1016/j.earscirev.2021.103503.

Sherman, R., R. Mullen, H. Li, Z. Fang, and Y. Wang. 2008. Spatial Patterns of Plant Diversity and Communities in Alpine Ecosystems of the Hengduan Mountains, Northwest Yunnan, China. *Journal of Plant Ecology* 1 (2): 117–36. https://doi.org/10.1093/jpe/rtn012.

Soltis, D. E., V. A. Albert, J. Leebens-Mack, C. D. Bell, A. H. Paterson, C. Zheng, D. Sankoff, C. W. de Pamphilis, P. K. Wall, and P. S. Soltis. 2009. Polyploidy and Angiosperm Diversification. *American Journal of Botany* 96 (1): 336–48. https://doi.org/10.3732/ajb.0800079.

Spicer, R. A., T. Su, P. J. Valdes, A. Farnsworth, F. Wu, G. Shi, T. E. V. Spicer, and Z. Zhou. 2021. Why 'the Uplift of the Tibetan Plateau' Is a Myth. *National Science Review* 8 (1): nwaa091. https://doi.org/10.1093/nsr/nwaa091.

Stadler, T. 2011. Mammalian Phylogeny Reveals Recent Diversification Rate Shifts. *Proceedings of the National Academy of Sciences USA* 108 (15): 6187–92. https://doi.org/10.1073/pnas.1016876108.

Stadler, T., A. Gavryushkina, R. C. M. Warnock, A. J. Drummond, and T. A. Heath. 2018. The Fossilised Birth-Death Model for the Analysis of Stratigraphic Range Data Under Different Speciation Modes. *Journal of Theoretical Biology* 447: 41–55. https://doi.org/10.1016/j.jtbi.2018.03.005.

Stadler, T., D. Kühnert, S. Bonhoeffer, and A. J. Drummond. 2012. Birth-Death Skyline Plot Reveals Temporal Changes of Epidemic Spread in HIV and Hepatitis c Virus (HCV).

Proceedings of the National Academy of Sciences USA 110 (1): 228–33. https://doi.org/10.1073/pnas.1207965110.

Steinbauer, M. J., R. Field, J.-A. Grytnes, P. Trigas, C. Ah-Peng, F. Attorre, H. J. B. Birks, et al. 2016. Topography-Driven Isolation, Speciation and a Global Increase of Endemism with Elevation. *Global Ecology and Biogeography* 25 (9): 1097–107. https://doi.org/10.1111/geb.12469.

Thompson, J., and S. Ramírez-Barahona. 2023. No Evidence for Angiosperm Mass Extinction at the Cretaceous-Paleogene (K-Pg) Boundary. *Biology Letters* 19 (9): 20230314. https://doi.org/10.1098/rsbl.2023.0314.

Vajda, V., and A. Bercovici. 2014. The Global Vegetation Pattern Across the Cretaceous-Paleogene Mass Extinction Interval: A Template for Other Extinction Events. *Global and Planetary Change* 122: 29–49. https://doi.org/10.1016/j.gloplacha.2014.07.014.

Vanneste, K., S. Maere, and Y. Van de Peer. 2014. Tangled up in Two: A Burst of Genome Duplications at the End of the Cretaceous and the Consequences for Plant Evolution. *Proceedings of the Royal Society B* 369 (1648): 20130353. https://doi.org/10.1098/rstb.2013.0353.

Vaughan, T. G. 2023. ReMASTER: Improved Phylodynamic Simulation for BEAST 2.7. *bioRxiv*, 1–3. https://doi.org/10.1101/2023.10.09.561485.

Xing, Y., and R. H. Ree. 2017. Uplift-Driven Diversification in the Hengduan Mountains, a Temperate Biodiversity Hotspot. *Proceedings of the National Academy of Sciences USA* 114 (17): E3444–51. https://doi.org/10.1073/pnas.1616063114.

Yin, A., and T. M. Harrison. 2000. Geologic Evolution of the Himalayan-Tibetan Orogen. *Annual Review of Earth and Planetary Sciences* 28 (1): 211–80. https://doi.org/10.1146/annurev.earth.28.1.211.

Zhan, X., Y. Zheng, F. Wei, M. W. Bruford, and C. Jia. 2011. Molecular Evidence for Pleistocene Refugia at the Eastern Edge of the Tibetan Plateau. *Molecular Ecology* 20 (14): 3014–26. https://doi.org/10.1111/j.1365-294X.2011.05144.x.

Zhang, D., Y. Zhang, D. E. Boufford, and H. Sun. 2009. Elevational Patterns of Species Richness and Endemism for Some Important Taxa in the Hengduan Mountains, Southwestern China. *Biodiversity and Conservation* 18: 699–716. https://doi.org/10.1007/s10531-008-9534-x.

Figures

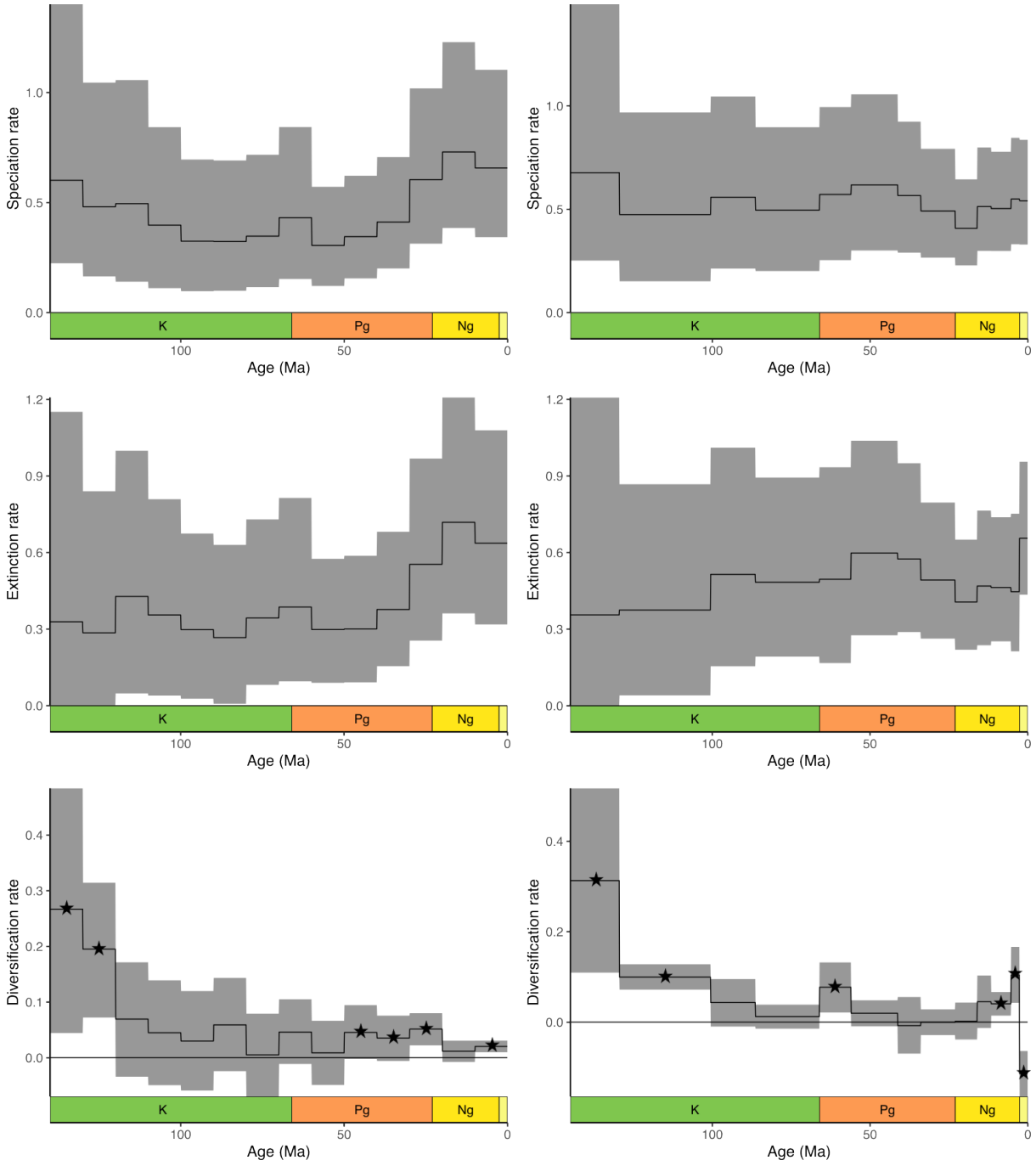

Fig. 1. Posterior distributions of speciation (top), extinction (middle) and net diversification (bottom) rates, estimated using the beta extant sampling probability prior. Analyses were conducted using equal 10My (left) and geological (right) time bins. The black lines show the median values, with the 95% highest posterior density (HPD) intervals shown in grey. Stars indicate bins for which at least 95% of the posterior distribution for diversification rate lies on the same side of the y-axis, showing clear signal for either positive or negative diversification. The geological time scale was added using the R package deeptime (Gearty 2023).

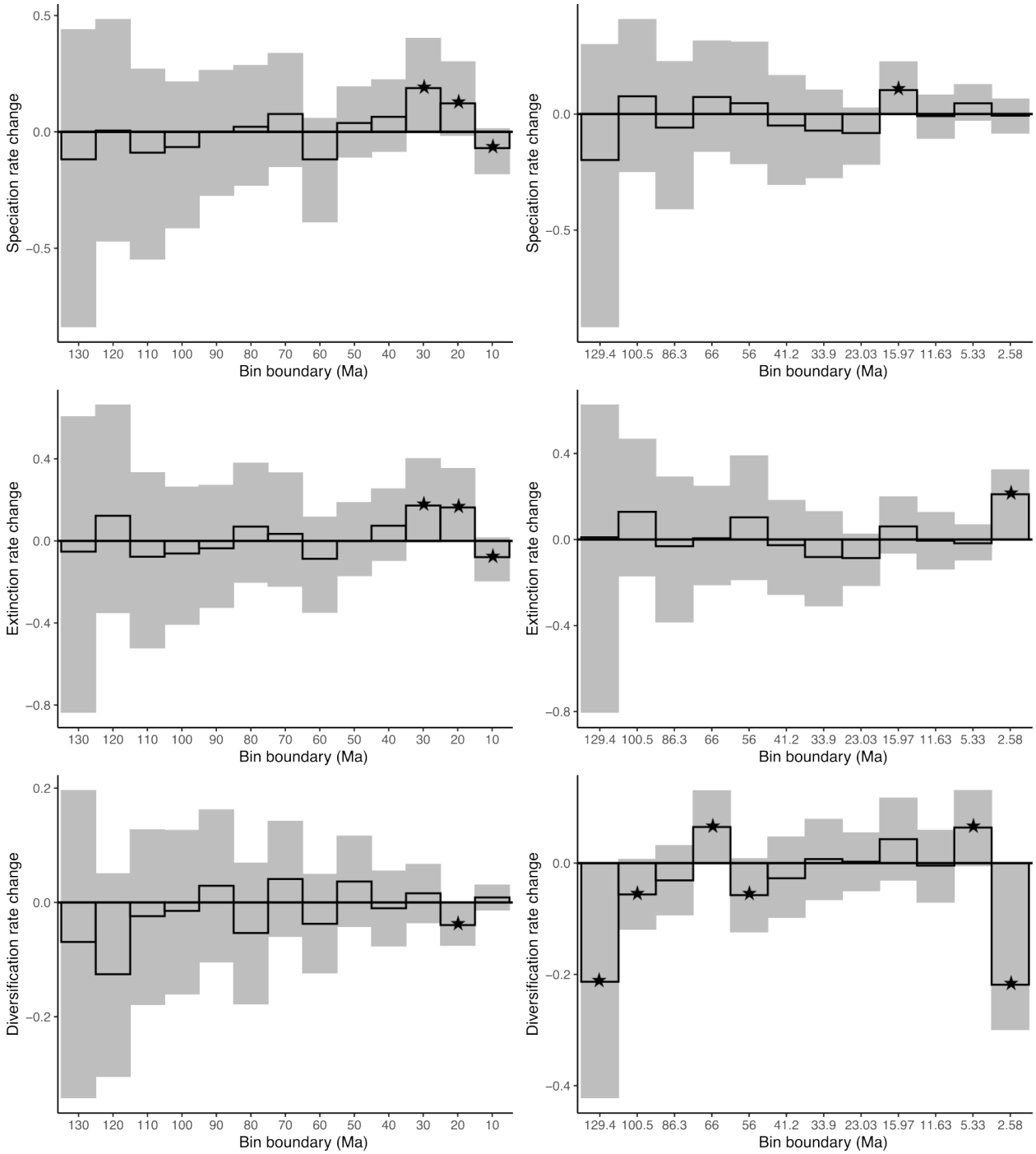

Fig. 2. Posterior distributions of change of rates between intervals. This distribution is obtained by calculating the difference between speciation (top), extinction (middle) and net diversification (bottom) rates for adjacent time bins in individual MCMC iterations. Analyses were conducted using equal 10My (left) and geological (right) time bins, with bin boundaries labelled from oldest to youngest (i.e. the direction of time is the same as Figure 1). The black bars show the median values, with the highest posterior density (95%) shown in grey. Stars indicate bins for which at least 95% of the posterior distribution lies on the same side of the y-axis, showing clear signal for either positive or negative rate change between adjacent time bins.

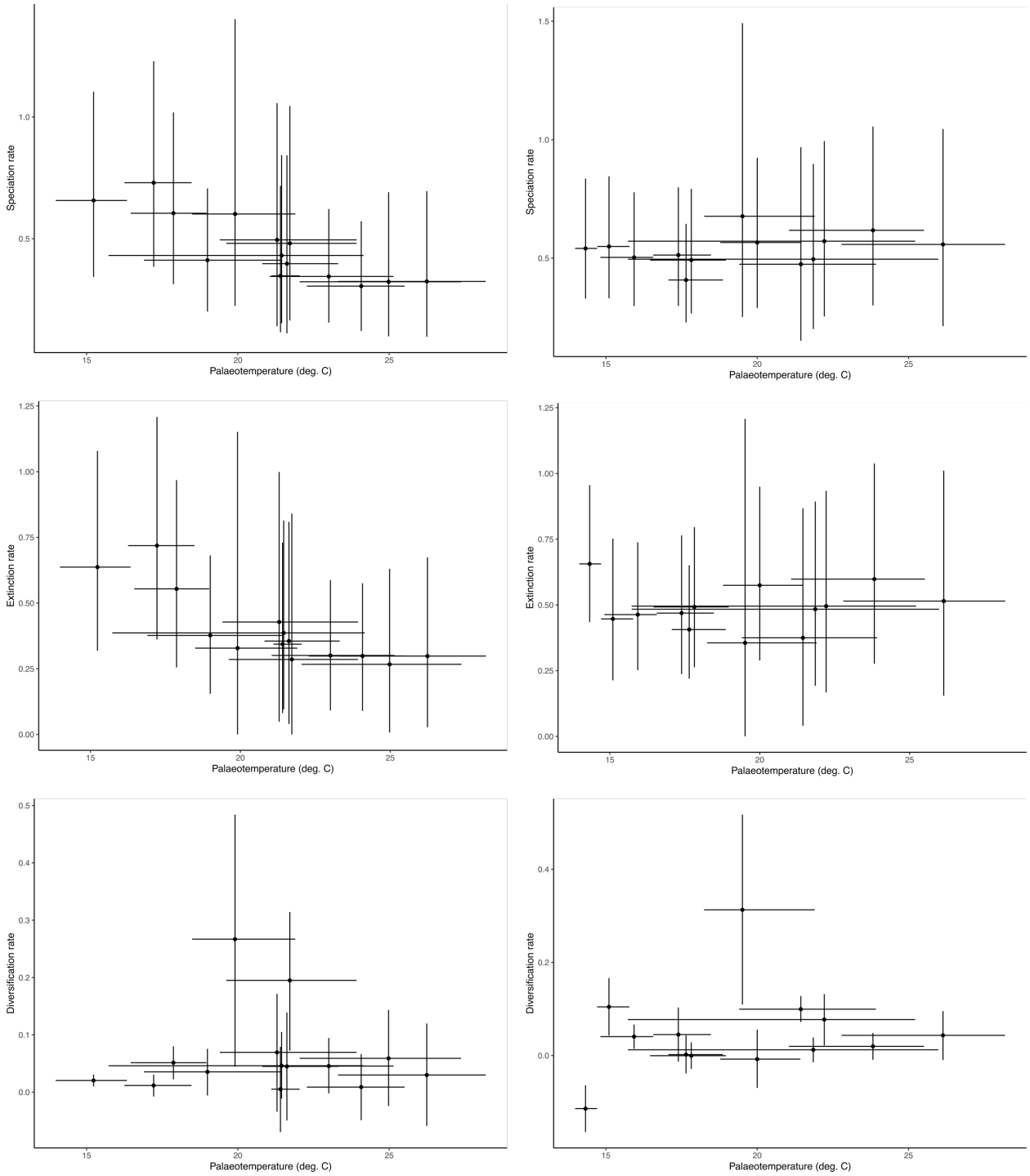

560

561 **Fig. 3.** Relationship between palaeotemperature and speciation (top), extinction (middle) and
562 net diversification (bottom) for equal time bins (left) and geological time bins (right). Horizontal
563 bars show the minimum and maximum temperatures within each time bin, with the point at the
564 mean. Vertical bars show the 95% HPD intervals, with the point at the median.

565

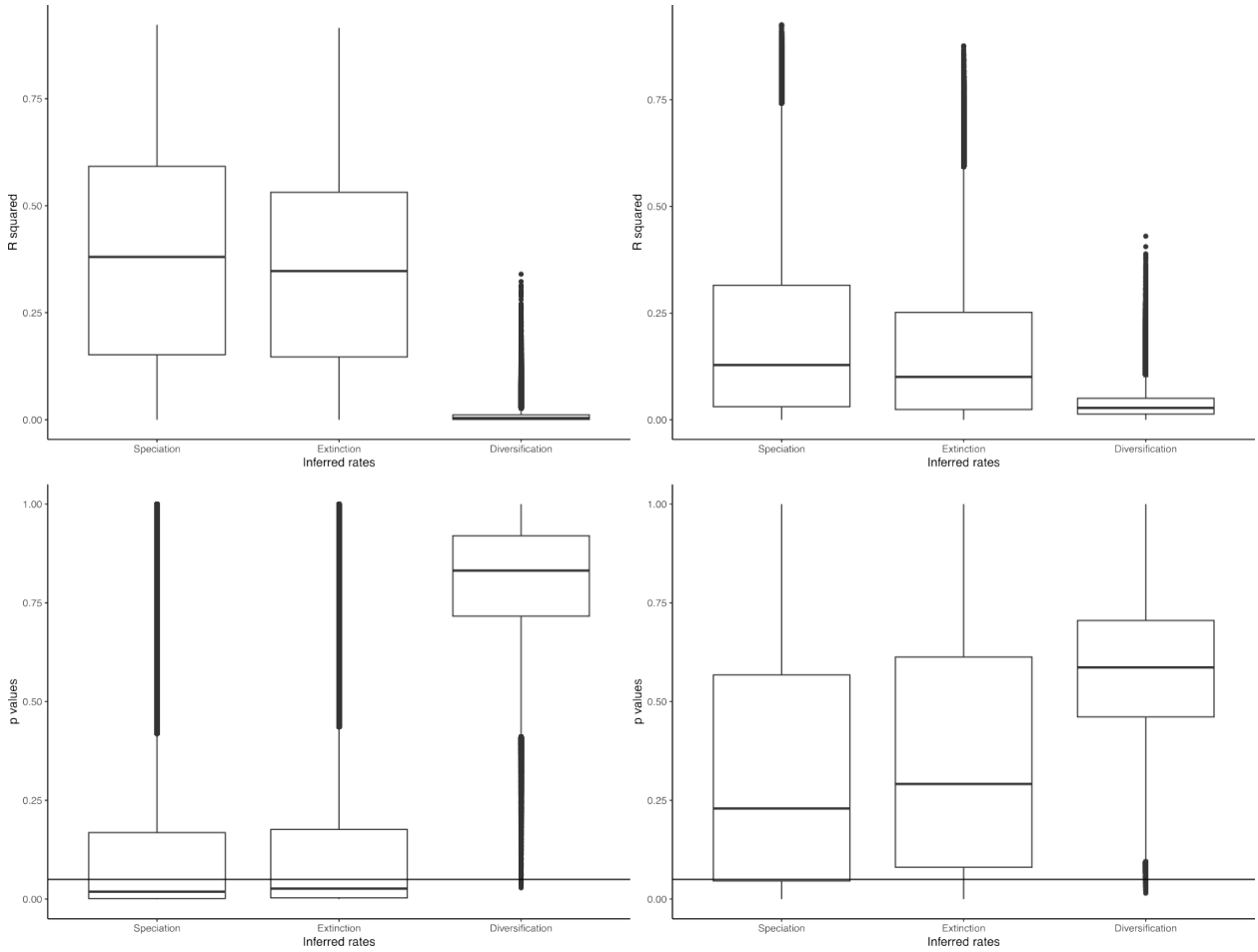

Fig. 4. Relationship between palaeotemperature and evolutionary rates for equal time bins (left) and geological time bins (right). Box plots show regression parameters estimated for evolutionary trajectory in each iteration (after burn-in) of the MCMC.

571 **Tables**

572 **Table 1.** The geological intervals used as time bins in the skyline analyses.

Interval	Start age (Mya)
Early Lower Cretaceous	145.0
Late Lower Cretaceous	129.4
Early Upper Cretaceous	100.5
Late Upper Cretaceous	86.3
Paleocene	66.0
Early Eocene	56.0
Late Eocene	41.2
Oligocene	33.9
Early Miocene	23.03
Middle Miocene	15.97
Late Miocene	11.63
Pliocene	5.333
Quaternary	2.58

573

574

Supplementary figures

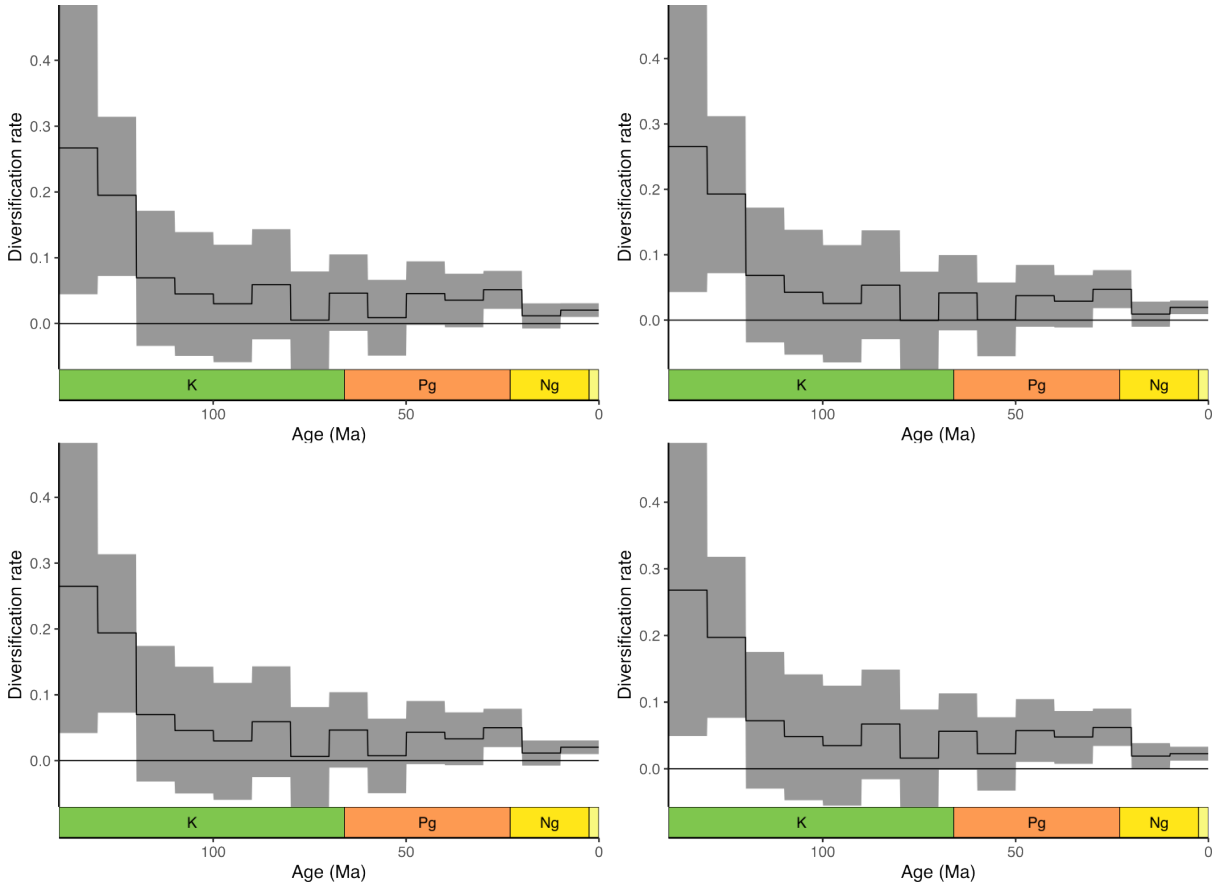

Fig. S1. Diversification rate estimates for analyses conducted using beta sampling prior (top left), sampling prior fixed at 0.5 (top right), sampling prior fixed at 0.3 (bottom left), and sampling prior fixed at 0.1 (bottom right).

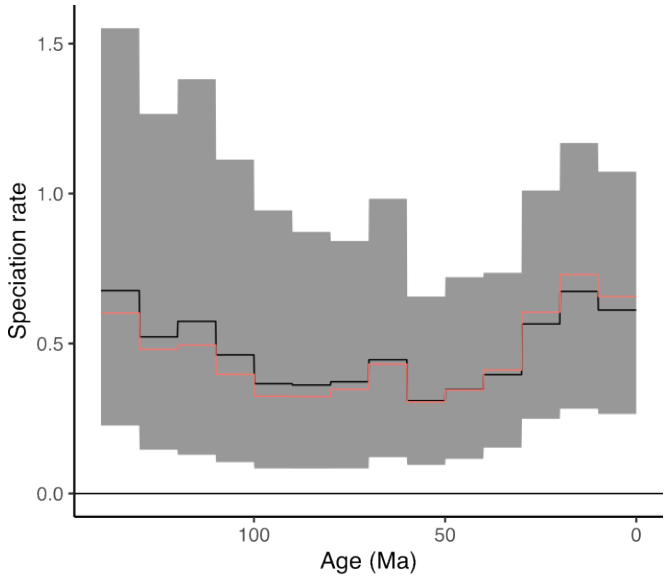
Speciation rate
1.5
1.0
0.5
0.0
100
50
0
Age (Ma)

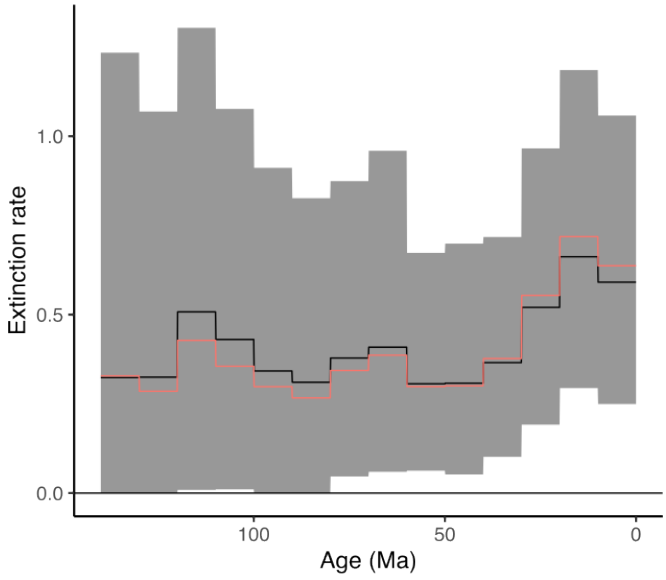
Extinction rate
1.0
0.5
0.0
100
50
0
Age (Ma)

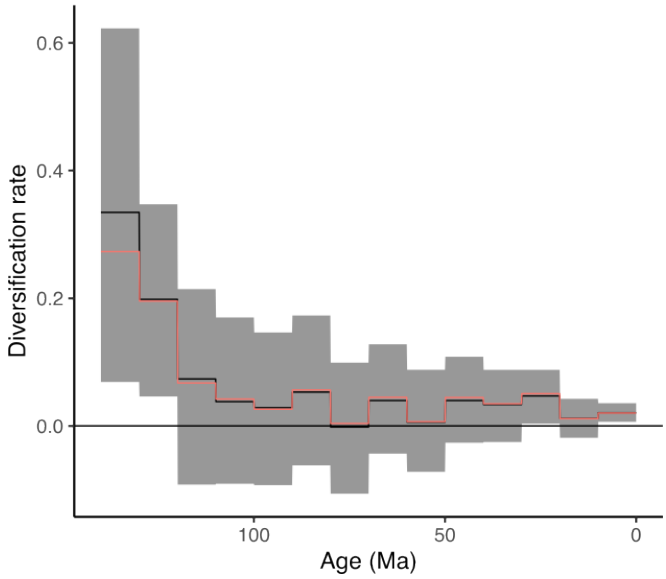
Diversification rate
0.6
0.4
0.2
0.0
100
50
0
Age (Ma)

Fig. S2. Posterior distributions of speciation (top), extinction (middle) and net diversification (bottom) rates from simulated phylogenies. 100 phylogenies were simulated using the median rates inferred from the equal-length time bin analysis (Fig. 1), and the skyline analysis was repeated on each of these; the figure here shows the posterior distribution based on sampling 200 iterations from each of these analyses. The black lines show the median values, with the 95% highest posterior density (HPD) intervals shown in grey. The median values from the original analysis, which were used to simulate the phylogenies, are shown in red.

Supplementary tables

Table S1. Summary of key diversification results.

Equal bins

Interval	Starting age (Mya)	Proportion of diversification posterior above 0	Proportion of positive diversification shifts into subsequent time bin
1	140	**0.9904**	0.3030
2	130	**0.9992**	0.0814
3	120	0.9055	0.3801
4	110	0.8254	0.4199
5	100	0.7433	0.6654
6	90	0.9154	0.1961
7	80	0.5534	0.7872
8	70	0.9399	0.1975
9	60	0.6191	0.8170
10	50	**0.9670**	0.381
11	40	**0.9539**	0.7316
12	30	**0.9998**	**0.0144**
13	20	0.8819	0.7833
14	10	**0.9999**	

Geological bins

Interval	Starting age (Mya)	Proportion of diversification posterior above 0	Proportion of positive diversification shifts into subsequent time bin
Early Lower Cretaceous	145.0	**0.9984**	**0.0242**
Late Lower Cretaceous	129.4	**1.0000**	**0.0395**
Early Upper Cretaceous	100.5	0.9461	0.1651
Late Upper Cretaceous	86.3	0.8170	**0.9750**
Paleocene	66.0	**0.9973**	**0.0438**
Early Eocene	56.0	0.9102	0.2361
Late Eocene	41.2	0.4071	0.5769
Oligocene	33.9	0.4882	0.5379
Early Miocene	23.03	0.5382	0.8725
Middle Miocene	15.97	0.9358	0.4467
Late Miocene	11.63	**0.9989**	**0.9677**

Pliocene	5.33	**0.9997**	**0.0000**
Quaternary	2.58	**0.0000**	

591

592

Table S2. Summary of speciation and extinction rate changes.

Equal bins

Interval	Starting age (Mya)	Proportion of positive speciation shifts into subsequent time bin	Proportion of positive extinction shifts into subsequent time bin
1	140	0.2948	0.4200
2	130	0.5128	0.7295
3	120	0.2763	0.3296
4	110	0.2837	0.3318
5	100	0.5032	0.3919
6	90	0.5887	0.7137
7	80	0.7966	0.6124
8	70	0.0699	0.1799
9	60	0.7280	0.4982
10	50	0.8316	0.8192
11	40	**0.9965**	**0.9824**
12	30	**0.9713**	**0.9882**
13	20	**0.0329**	**0.0329**

Geological bins

Interval	Starting age (Mya)	Proportion of positive speciation shifts into subsequent time bin	Proportion of positive extinction shifts into subsequent time bin
Early Lower Cretaceous	145.0	0.1624	0.5142
Late Lower Cretaceous	129.4	0.7149	0.8354
Early Upper Cretaceous	100.5	0.3264	0.4159
Late Upper Cretaceous	86.3	0.7679	0.5227
Paleocene	66.0	0.6558	0.7752
Early Eocene	56.0	0.3106	0.3917
Late Eocene	41.2	0.1885	0.2126
Oligocene	33.9	0.0560	0.0537

Early Miocene	23.03	**0.9857**	0.8430
Middle Miocene	15.97	0.4176	0.4664
Late Miocene	11.63	0.9066	0.3354
Pliocene	5.33	0.4170	**0.9998**

593